Early stage of nanodroplet impact on solid wall

Kazumichi Kobayashi, Kazuki Konno, Hisao Yaguchi, Hiroyuki Fujii, Toshiyuki Sanada, and Masao Watanabe

Citation: Physics of Fluids **28**, 032002 (2016); doi: 10.1063/1.4942874
View online: http://dx.doi.org/10.1063/1.4942874
View Table of Contents: http://scitation.aip.org/content/aip/journal/pof2/28/3?ver=pdfcov
Published by the AIP Publishing

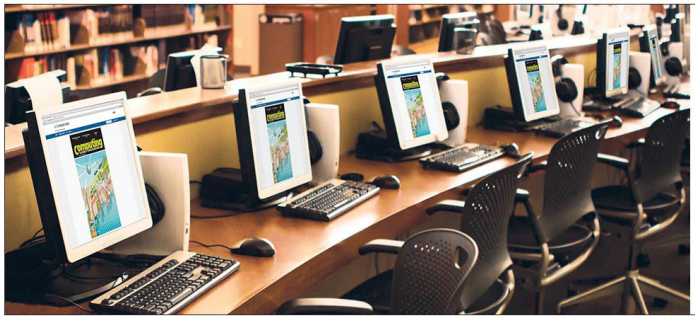

PHYSICS OF FLUIDS **28**, 032002 (2016)

Early stage of nanodroplet impact on solid wall

Kazumichi Kobayashi,[1,a)] Kazuki Konno,[1] Hisao Yaguchi,[2] Hiroyuki Fujii,[1] Toshiyuki Sanada,[3] and Masao Watanabe[1]
[1]*Division of Mechanical and Space Engineering, Faculty of Engineering, Hokkaido University, Kita 13 Nishi 8, Kita-ku, Sapporo, Hokkaido 060-8628, Japan*
[2]*Department of Mechanical Engineering, National Institute of Technology, Gunma College, Toriba-machi, Maebashi 371-8530, Japan*
[3]*Department of Mechanical Engineering, Shizuoka University, 3-5-1 Johoku, Naka-ku, Hamamatsu, 432-8561, Japan*

(Received 17 July 2015; accepted 15 February 2016; published online 4 March 2016)

In this study, we investigated nanodroplet spreading at the early stage after the impact using molecular dynamics simulations by changing the magnitude of the intermolecular force between the liquid and wall molecules. We showed that the droplet deformation after the impact greatly depends on the intermolecular force. The temporal evolution of the spreading diameters was measured by the cylindrical control volume for several molecular layers in the vicinity of the wall. At the early stage of the nanodroplet impact, the normalized spreading radius of the droplet is proportional to the square root of the normalized time, $\hat{t}$. This result is understood by the geometrical consideration presented by Rioboo *et al.* ["Time evolution of liquid drop impact onto solid, dry surfaces," Exp. Fluids **33**, 112–124 (2002)]. In addition, we found that as the intermolecular force between the liquid and wall becomes stronger, the normalized spreading diameter of the first molecular layer on the wall remains less dependent on the impact velocity. Furthermore, the time evolution of the droplet spreading changes from $\sqrt{\hat{t}}$ to $\log \hat{t}$ with time. © *2016 AIP Publishing LLC.* [http://dx.doi.org/10.1063/1.4942874]

I. INTRODUCTION

Numerous studies of droplet spreading after droplet impact have been conducted by observing the millimeter or micrometer droplet impact,[1–4] to share fruitful knowledge with us. At the early stage of droplet impact, the spreading radius R was found to be given by

$$\frac{R(t)}{R_0} \sim \sqrt{\hat{t}}, \quad \text{where } \hat{t} = \frac{t}{t^*}, \tag{1}$$

where R_0 is the initial radius of the droplet, t is the time, and t^* is the reference time defined as $t^* = D_0/V_i$, where V_i is the impact velocity of the droplet and $D_0(=2R_0)$ is the droplet diameter. Rioboo *et al.*[2] experimentally showed that Eq. (1) arises from the geometric considerations of droplet spreading at the early stage (for $\hat{t} \leq 0.1$), which they called as the *kinematic phase*. Furthermore, they showed that Eq. (1) is independent of $\mathrm{We}(=\rho_\ell D_0 V_i^2/\gamma)$, $\mathrm{Re}(=D_0 V_i/\nu_\ell)$, and wettability of the wall within the kinematic phase, where ρ_ℓ is the density of the liquid, γ is the surface tension, and ν_ℓ is the kinematic viscosity of the liquid. This result by Rioboo *et al.* leads to the conclusion that Eq. (1) is independent of the physical properties of the liquid and the wall, therefore, the obtained description of the spreading radius should be quite general. Conversely, Biance *et al.*[5] showed that Eq. (1) arises from the inertia–capillary balance while neglecting the viscosity at the first step of the spreading. They concluded that the surface force plays a dominant roll in the first step of droplet spreading.

a)Author to whom correspondence should be addressed. Electronic mail: kobakazu@eng.hokudai.ac.jp

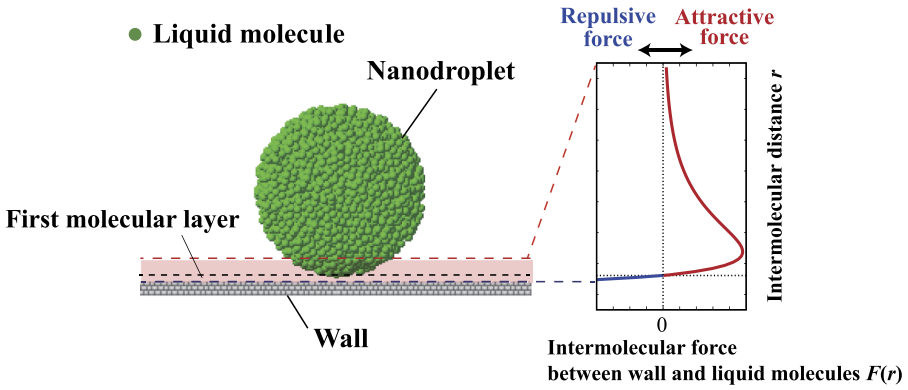

FIG. 1. Schematic of nanodroplet impact. Green spheres denote the liquid molecules. The right graph shows the intermolecular force between liquid and wall molecules. As the droplet becomes smaller, the influence of the wall on the droplet deformation becomes larger.

Taking advantage of the ease of treating the liquid–wall interaction, several studies of nanodroplet impact were conducted using molecular dynamics (MD) simulation.[6–14] Recently, Koplik and Zhang[12] investigated the behaviors of nanodroplets consisting of short chains of Lennard-Jones liquids after impact with the solid surface, and Zhang *et al.*[13] studied the influence of wettability and roughness of solid surfaces for nanodroplet impact. From these studies, detailed spreading dynamics due to the nanodroplet impact have been clarified. Furthermore, some studies[7,8,10,11,13] showed that the droplet spreading obeys Eq. (1). However, the detailed mechanism underlying the spreading radius behavior described by Eq. (1) has not been clarified.

We should notice that nanodroplet spreading is more affected by the intermolecular force between the wall surface and liquid molecules than the millimeter droplet because the range of influence of intermolecular forces (mainly attractive force) in the vicinity of the wall surface is several nanometers as shown in Fig. 1. Thus, the first molecular layer of the droplet on the wall and also the several layers are affected by the intermolecular force of the wall, possibly leading to the variation of the droplet deformation due to the impact. Several studies have been conducted to study the influence of intermolecular force of the wall surface on the nanodroplet spreading and contact line development for nanodroplets.[8–10,12,13] However, no studies have investigated the spreading dynamics for the several molecular layers in the vicinity of the wall, and the difference between the microscopic and macroscopic views of the droplet spreading and the variation of the droplet deformation under the influence of the wall have not been systematically clarified.

To shed light on the problems described above, we study the influence of the intermolecular force of the wall at the early stage of nanodroplet spreading using molecular dynamics simulation for simple molecules. We use Ar to represent both liquid and vapor, and Pt for solid wall. We investigate the influence of the intermolecular force of wall surface on the spreading dynamics of nanodroplet by changing the magnitude of the intermolecular force between Ar and Pt. Furthermore, we elucidate the origin of Eq. (1) for nanodroplet spreading and discuss the characteristic behaviors of the spreading dynamics of nanodroplet.

II. METHOD

The simulation system consisted of a simulation box with dimensions $L_x \times L_y \times L_z$, where $L_x = 43.3$ nm, $L_y = 43.2$ nm, and $L_z = 40.0$ nm, as shown in Fig. 2(a). Periodic boundary conditions were imposed on the simulation system in x and y directions. For z direction, a miller boundary was imposed at the edge of the simulation system.

For the intermolecular potential of Ar–Ar interactions at 85 K, we used a 12-6 type Lennard–Jones potential,

$$\phi_{\mathrm{Ar}}(r) = 4\epsilon_{\mathrm{Ar}}\left[\left(\frac{\sigma_{\mathrm{Ar}}}{r}\right)^{12} - \left(\frac{\sigma_{\mathrm{Ar}}}{r}\right)^{6}\right], \tag{2}$$

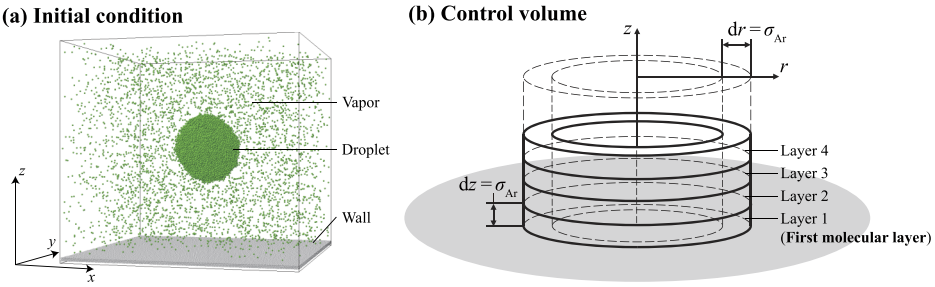

FIG. 2. Simulation configuration: (a) initial condition of the present study; (b) control volume of the present study.

where the particle radius σ_{Ar} is 3.405 Å, the potential depth $\epsilon_{\mathrm{Ar}}/k_b$ is 119.8 K, and k_b is the Boltzmann constant. The total number of Ar molecules was 26 770, and the droplet diameter D_0 was 12.60 nm. Newton's equations of motion for the molecules in the system were solved by the leap–frog method. The time step was 5 fs and the cutoff radius was 15 Å.

For the intermolecular potential of the Ar–Pt interactions, we used the following intermolecular potential:

$$\phi_W(r) = 4\epsilon_W\left[\left(\frac{\sigma_W}{r}\right)^{12} - \beta\left(\frac{\sigma_W}{r}\right)^{6}\right], \tag{3}$$

with

$$\sigma_W = \frac{(\sigma_{\mathrm{Ar}} + \sigma_{\mathrm{Pt}})}{2}, \qquad \epsilon_W = \alpha\sqrt{\epsilon_{\mathrm{Ar}} \cdot \epsilon_{\mathrm{Pt}}}, \tag{4}$$

where $\sigma_{\mathrm{Pt}} = 2.475$ Å and $\epsilon_{\mathrm{Pt}}/k_b = 6048$ K, respectively. Previous MD simulations[10,13,15,16] have shown that the contact angle changes with changes in α and β. In this study, the value of β is fixed as $\beta = 1.0$. In contrast, the value of α is determined

$$\epsilon^* = \frac{\epsilon_W}{\epsilon_{\mathrm{Ar}}} = \alpha\sqrt{\frac{\epsilon_{\mathrm{Pt}}}{\epsilon_{\mathrm{Ar}}}}, \tag{5}$$

where $\epsilon^* = 7.1$ ($\alpha = 1.000$), 1.0 ($\alpha = 0.141$), and 0.05 ($\alpha = 0.007$) are used in this simulation. Here, it is emphasized that $\epsilon^* = 1.0$ means that the potential for liquid–wall interaction is the same as that for the liquid–liquid interactions. From the previous MD simulations,[10,15,16] the static contact angles for $\epsilon^* = 7.1$, 1.0, and 0.05 become about 0°, 0°, and 180°, respectively.

The following harmonic oscillator potential was used to represent the interaction of the wall molecules:

$$\phi_H = \frac{1}{2}K(r - r_0)^2, \tag{6}$$

where K is the spring constant ($K = 46.8$ N/m) and $r_0 = 0.2774$ nm. The spatial arrangement of wall molecules follows the fcc(1 1 1) crystal lattice. The wall consists of the 3 layers of Pt molecules. Other two layers of Pt were inserted to control the temperature of the solid wall (85 K). These two layers do not interact with the argon molecules. The total number of Pt molecules is 140 400. A more detailed description of the methodology is provided in the previous study.[17]

In this simulation, the droplet deformation due to the impact can be considered as an axis-symmetric phenomenon. Hence, a cylinder-shaped control volume was used to investigate the density and velocity fields in the droplet, as shown in Fig. 2(b). The thickness dr and height dz of each control volume are σ_{Ar}. From the bottom up, we referred to the control volumes as *Layer* 1, *Layer* 2, *Layer* 3, and *Layer* 4. These layers were within the range of cutoff radius of wall molecules. We investigated the droplet spreading on a molecular scale. To obtain accurate values of macroscopic properties such as density and velocity, we performed multiple simulations to obtain ensemble averaging.

We performed simulations of vapor-liquid droplet equilibrium using the mass center position control method[18] at 85 K without the solid wall to obtain equilibrated initial conditions for the

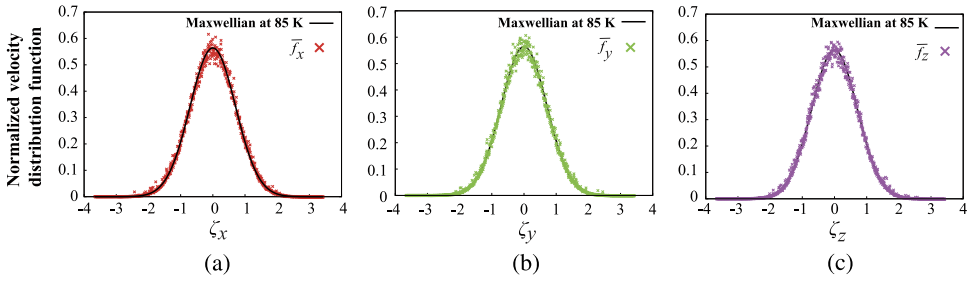

FIG. 3. Velocity distribution functions of liquid molecules after the equilibrium simulation: (a) x direction, (b) y direction, and (c) z direction.

simulations. Figure 3 shows the normalized velocity distribution function of liquid molecules after the equilibrium simulation for the x, y, and z velocity components. The solid lines are given by the normalized Maxwell velocity distribution function at 85 K,

$$\bar{f} = \bar{f}_x \bar{f}_y \bar{f}_z = \frac{1}{(2\pi R_g T_\ell)^{3/2}} \exp\left(-\frac{\xi_x^2 + \xi_y^2 + \xi_z^2}{2R_g T_\ell}\right).$$

The abscissa is the normalized molecular velocity $\zeta_i = \xi_i/\sqrt{2R_g T_\ell}$, where R_g is the gas constant, T_ℓ is the liquid temperature, the subscript i (=x, y, and z) denotes the Cartesian directions, and the ordinate is the normalized velocity distribution function. As can be seen from Fig. 3, the simulation results agree with the Maxwell velocity distribution, thus, droplet molecules reached an equilibrium state at 85 K following our equilibrium simulations.

Following the equilibration of the system, we inserted the wall molecules and set the initial velocity (average velocity of molecules), V_0, for the droplet molecules to be toward the wall. In this simulation, the initial velocities are 100, 200, 250, 300, and 350 m/s. The corresponding impact velocities, V_i, measured at the instance of the droplet impact are 92, 188, 235, 282, and 330 m/s, respectively.

The values of the Weber numbers are from We = 1.04 for V_i = 92 m/s to We = 13.39 for V_i = 330 m/s, where the liquid density and the surface tension are estimated using the data of the previous MD simulation.[18] Since the nanodroplet diameter is 12.60 nm, the effect of surface tension becomes higher than that of inertia force, which leads to the suppression of the droplet deformation. Thus, in this simulation, we carried out the high-speed droplet impact to observe the droplet deformation.

III. RESULTS

A. Influence of intermolecular force of wall on nanodroplet spreading

Figure 4 shows the density profiles of the droplet impact with V_i = 92 m/s for (a) ϵ^* = 7.1, (b) ϵ^* = 1.0, and (c) ϵ^* = 0.05, respectively. For ϵ^* = 7.1, we can see that the droplet deforms and spreads to the radial direction with time. When $\hat{t}$ is 0.25, a thin film is generated on the wall (Fig. 4(i)), followed by the formation of a high density region on the wall due to the presence of a strong intermolecular force between the wall and liquid (Fig. 4(ii)).

While a similar spreading process is observed in the case of ϵ^* = 1.0, the high density region is not formed in the vicinity of the wall (Fig. 4(iii)). At the normalized time $\hat{t}$ = 1.0, the droplet shapes for ϵ^* = 7.1 and 1.0 are almost the same: the heights of droplets with ϵ^* = 7.1 and 1.0 are 5.7 nm and 5.4 nm, respectively.

For ϵ^* = 0.05, the liquid density on the wall becomes smaller than that of the bulk liquid due to the weak intermolecular interaction with the wall (Fig. 4(iv)). The minimum droplet height reaches around $\hat{t}$ = 0.75, followed by a rebound to greater heights. Such a rebound process for the small value of ϵ^* was also observed in the previous MD simulations.[10,14]

Next, we investigate the spreading diameter of the molecular layers (Layers 1–4 shown in Fig. 4) using the control volumes as shown in Fig. 2(b). Figure 5(a) shows the temporal evolution of

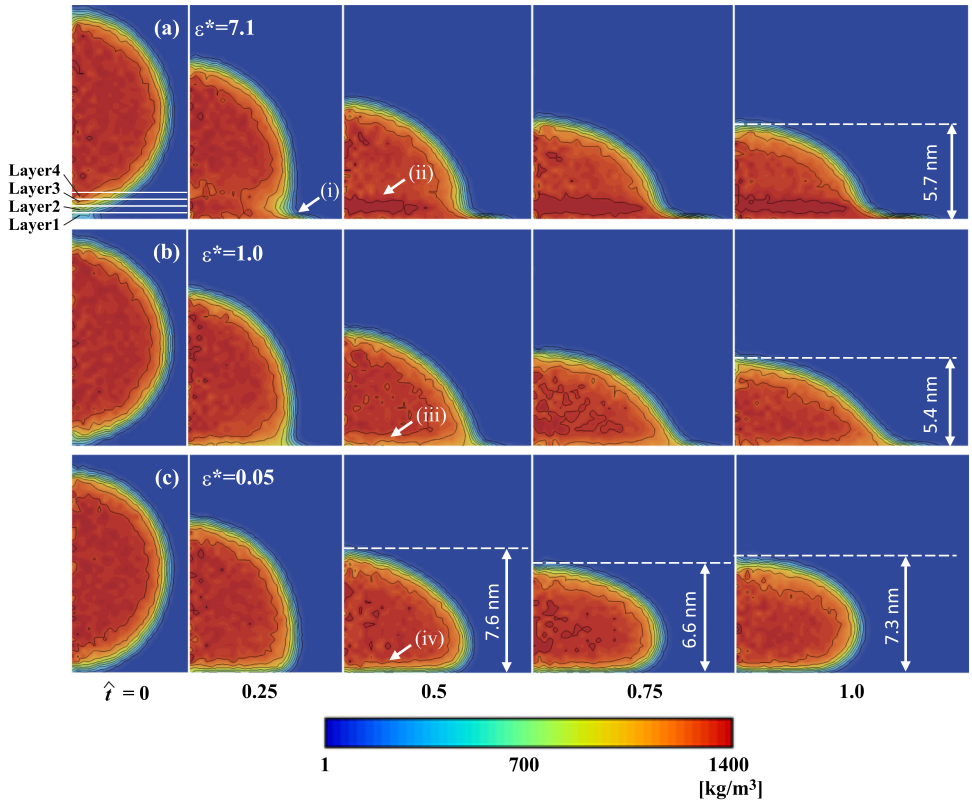

FIG. 4. Density profiles of the nanodroplet ($D_0 = 12.60$ nm) impact at $V_i = 92$ m/s for (a) $\epsilon^* = 7.1$, (b) $\epsilon^* = 1.0$, and (c) $\epsilon^* = 0.05$.

droplet spreading in Layer 1 at $V_i = 92$ m/s. The red, blue, and green circles correspond to data for $\epsilon^* = 0.05$, 1.0, and 7.1, respectively. The vapor–liquid interface is defined as the position with the density that is 25% of the liquid density.[10] The droplet spreading in Layer 1 for $\hat{t} < 0.05$ follows the same trend for all ϵ^*. Figure 5(b) shows the log–log plot of the data in Fig. 5(a). The inspection of the figure shows that the time evolution of the droplet spreading is described by $R(t)/R_0 \sim \sqrt{\hat{t}}$ at the early stage of impact.

Rioboo *et al.*[2] showed that, for a millimeter droplet, the spreading diameter is independent of the wettability of the wall within the kinematic phase. Based on the geometric considerations of droplet spreading in the kinematic phase, Rioboo *et al.* also derived the following equation[2] shown as a solid line in Fig. 5(a):

$$\frac{R(t)}{R_0} = 2\sqrt{\hat{t}}\sqrt{1-\hat{t}}, \tag{7}$$

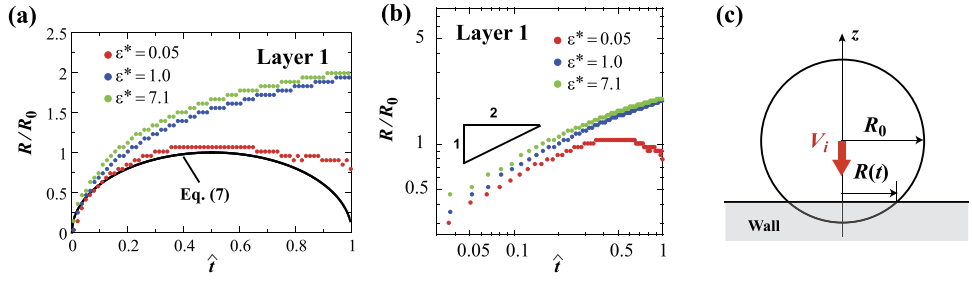

FIG. 5. Time evolutions of droplet spreading of Layer 1 for $\epsilon^* = 0.05, 1.0$, and 7.1; (b) log–log plot of (a); and (c) schematic of the movement of the contact line during the kinematic phase derived by Rioboo *et al.*[2] (Equation (7)).

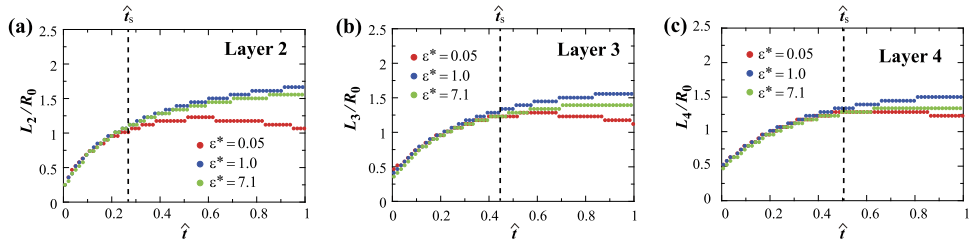

FIG. 6. Time evolutions of the droplet spreading of each Layer for $\epsilon^* = 0.05, 1.0$, and 7.1: (a) Layer 2; (b) Layer 3; and (c) Layer 4.

where schematic of $R(t)/R_0$ in the above equation is shown in Fig. 5(c). Figure 5(a) shows that the solid line and numerical results within $\hat{t} < 0.05$ coincide; the early stage of the nanodroplet spreading is strongly governed by the geometrical shape of the droplet. This is the origin of the $R(t)/R_0 \sim \sqrt{\hat{t}}$ relationship for the nanodroplet. Furthermore, we find that the time evolution of the droplet spreading with ϵ^* of 0.05 is well described by Eq. (7). From the above discussion, we can define that the kinematic phase of the present study is about $\hat{t} < 0.05$.

Figure 6 shows the time evolutions of droplet spreading in Layers 2–4 at $V_i = 92$ m/s. The ordinate is the radius of the droplet in each layer, $L_i(t)/R_0$, where i is the layer number, $i = 2$, 3, and 4, respectively. As the layer number increases, that is, as the layer departs further from the wall, the duration that the time evolution of the spreading radius coincide with each other in spite of the difference of ϵ^* becomes longer (for Layers 2–4, the time are $\hat{t} = 0.28$, 0.42, and 0.50, respectively). We define this time as $\hat{t}_s$ as shown in Fig. 6. The results of Fig. 6 show that the influence of the liquid–wall intermolecular force gradually appears from the bottom of the droplet. The droplet spreading is governed by only the liquid properties at $\hat{t} < \hat{t}_s$.

At the time $\hat{t} < \hat{t}_s$, we model the droplet spreading in Layers 2–4 on the following equation using the nonlinear least square method:

$$\frac{L_i(t)}{R_0} = A\hat{t}^B + C. \tag{8}$$

The obtained values of B for Layers 2–4 are 0.71, 0.78, and 0.74, respectively. In Eq. (8), the correlation coefficient for Layer 2 is 0.971, that for Layer 3 is 0.966 and that for Layer 4 is 0.968, respectively. Hence, the droplet spreading in Layers 2–4 does not follow $L_i(t)/R_0 \sim \sqrt{\hat{t}}$. We conclude that only Layer 1 obeys $R(t)/R_0 \sim \sqrt{\hat{t}}$.

We next study the velocity fields of the droplet impact at $V_i = 92$ m/s to investigate the difference of the droplet spreading processes due to the influence of the wall at $\hat{t} > \hat{t}_s$ in Layers 1–4. Figure 7 shows the velocity and density fields inside the droplet at $\hat{t} = 0.5$: (a) $\epsilon^* = 7.1$, (b) $\epsilon^* = 1.0$,

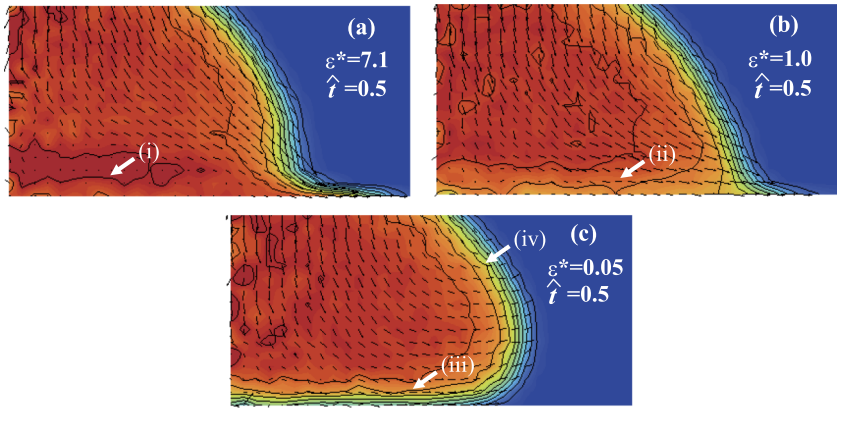

FIG. 7. Velocity and density fields inside the nanodroplet impact at $\hat{t} = 0.5$ (a) $\epsilon^* = 7.1$, (b) $\epsilon^* = 1.0$, and (c) $\epsilon^* = 0.05$. The impact velocity is $V_i = 92$ m/s.

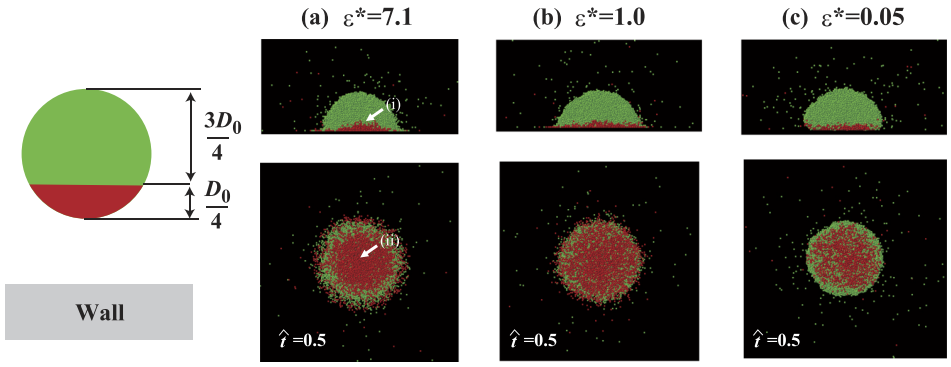

FIG. 8. Snapshots of nanodroplet impact at $\hat{t} = 0.5$ (a) $\epsilon^* = 7.1$, (b) $\epsilon^* = 1.0$, and (c) $\epsilon^* = 0.05$. The impact velocity is $V_i = 92$ m/s. As shown in the schematic of the left hand side, the under droplet molecules are characterized as red and upper droplet molecules are green.

and (c) $\epsilon^* = 0.05$. For $\epsilon^* = 7.1$, the observed droplet has a zero velocity region at the center of the droplet (Fig. 7(i)) in the vicinity of the wall due to the strong intermolecular force of the wall. However, for $\epsilon^* = 0.05$ and 1.0, the liquid in the vicinity of the wall exhibits a tangential velocity and a droplet spreads (Figs. 7(ii) and 7(iii)). The result of $\epsilon^* = 1.0$ is in good agreement with the velocity fields inside the millimeter droplet.[4] The liquid of the droplet edge also shows an upward velocity in the case of $\epsilon^* = 0.05$ (Fig. 7(iv)).

To visualize the molecular motion at $\hat{t} = 0.5$, we show the snapshots of liquid molecules in Fig. 8. In this figure, we use the red and green molecules, as shown in the schematic figure on the left-hand side of Fig. 8, to illustrate the motion of the lower droplet molecules. The upper figures are the cross sectional side view of the droplet, and the lower figures are the bottom view. The inspection of the figures shows that, for $\epsilon^* = 7.1$, a large number of red molecules remain around the center of the droplet (Figs. 8(i) and 8(ii)). This means that the molecules around the center of the droplet are forcibly restrained due to the strong intermolecular force between the liquid and wall, which leads to the zero velocity field as shown in Fig. 7(i). However, as ϵ^* decreases, the mobility of molecules increases; hence, the zero velocity region disappears, and the liquid velocity is observed around the center of the droplet.

As shown in Figs. 7 and 8, the molecules in the vicinity of the wall are strongly affected by the intermolecular force between the wall and liquid that changes the velocity fields inside the nanodroplet after the time $\hat{t}_s$. Thus, the difference in the intermolecular force between the droplet and wall leads to changes in the droplet deformation.

B. Influence of impact velocity on nanodroplet spreading

We now discuss the influence of impact velocity on nanodroplet spreading. Figure 9 shows the density profiles of the droplet impact for $V_i = 288$ m/s with (a) $\epsilon^* = 7.1$, (b) $\epsilon^* = 1.0$, and (c) $\epsilon^* = 0.05$. For all cases, the droplet spreads and the heights of all droplets at $\hat{t} = 1.0$ become smaller than those at the impact velocity $V_i = 92$ m/s (Fig. 4). In our simulation, the shock wave propagation inside the droplet[19] could not be observed while the decrease in the liquid density could be observed as shown in Fig. 9. The densities in the bulk liquid at $\hat{t} = 1.0$ decrease relative to their initial values (Figs. 9(i)–9(iii)). We confirmed that this is caused by the increase in the temperature inside the bulk liquid relative to the initial temperature (85 K) due to the high-speed impact. However, for $\epsilon^* = 7.1$, the high density region in the vicinity of the wall is still formed due to the high intermolecular force of the wall (Fig. 9(iv)).

Next, we investigate the dimensionless similarity of the spreading for the various impact velocities. Figure 10 shows the temporal evolution of droplet spreading in Layer 1 for various impact velocities with (a) $\epsilon^* = 0.05$, (b) $\epsilon^* = 1.0$, and (c) $\epsilon^* = 7.1$. The impact velocities are 92, 188, 235, 282, and 330 m/s, respectively. For $\epsilon^* = 0.05$ and $\epsilon^* = 1.0$, we found the characteristic time $\hat{t}_w$. The temporal evolution of the spreading at all impact velocities follows the same trend when $\hat{t} < \hat{t}_w$

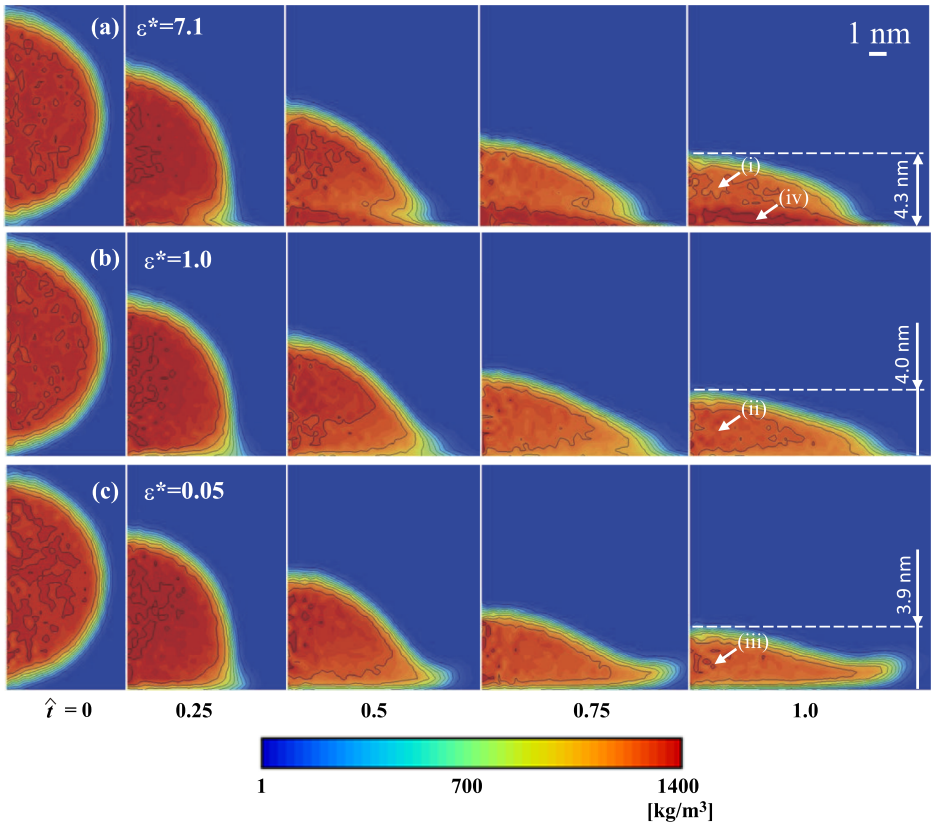

FIG. 9. Density profiles of the nanodroplet ($D_0 = 12.60$ nm) impact at $V_i = 288$ m/s, (a) $\epsilon^* = 7.1$, (b) $\epsilon^* = 1.0$, and (c) $\epsilon^* = 0.05$.

while the radius increases with the increase in the impact velocity when $\hat{t} > \hat{t}_w$. We also found that this time, $\hat{t}_w$, strongly depends on the intermolecular force: $\hat{t}_w$ increases with the increase in ϵ^*; $\hat{t}_w$ for $\epsilon^* = 0.05$ is 0.2 and $\hat{t}_w$ for $\epsilon^* = 1.0$ is 0.49. Rioboo *et al.*[2] have shown that the influence of the impact velocity appears for $0.1 < \hat{t} < 1.0$ in the case of the millimeter droplet. However, we find that for strong liquid–wall intermolecular force represented by $\epsilon^* = 7.1$, the temporal evolution of the droplet spreading in Layer 1 is independent of the impact velocity within $\hat{t} \leq 1.0$, in which dimensionless similarity of the spreading can thus be achieved. The same tendency was observed in the results of Zhang *et al.*[13] We conclude that the spreading of the first molecular layer (Layer 1) of the nanodroplet is strongly depend on the liquid-wall intermolecular force.

Here, in the case of $\epsilon^* = 7.1$, from Fig. 10(c), we can assume that the time evolution of the droplet spreading for $\hat{t} < 0.3$ is described by

$$\frac{R(t)}{R_0} = A'\sqrt{\hat{t}}, \quad \text{for} \quad \hat{t} < 0.3, \tag{9}$$

where $A' = 2.2$. Also, we find that Eq. (9) can describe the droplet spreading at the early stage of the droplet impact for $\epsilon^* = 0.05$ and 1.0 as shown in Figs. 10(a) and 10(b). A similar power law of the droplet spreading is observed regardless of the difference of ϵ^* at the early stage. This result also agrees with the millimeter droplet spreading.[2] However, as the value of ϵ^* becomes smaller, Eq. (9) can describe the droplet spreading for a shorter duration. After this duration, we cannot find the explicit power law of the droplet spreading for either $\epsilon^* = 0.05$ or 1.0 because the droplet spreading shows a strong dependence on the impact velocity.

Figure 10(d) shows the time evolution of the vapor–liquid interface velocity in Layer 1 (spreading velocity), V_r, in the case of $\epsilon^* = 7.1$ obtained from the ensemble averages of the molecules. The data of impact velocities 92, 188, and 282 m/s are shown. Examination of Fig. 10(d) shows that the dimensionless spreading velocities, $V_r(t)/V_i$, for all impact velocities, follow the same trend. In

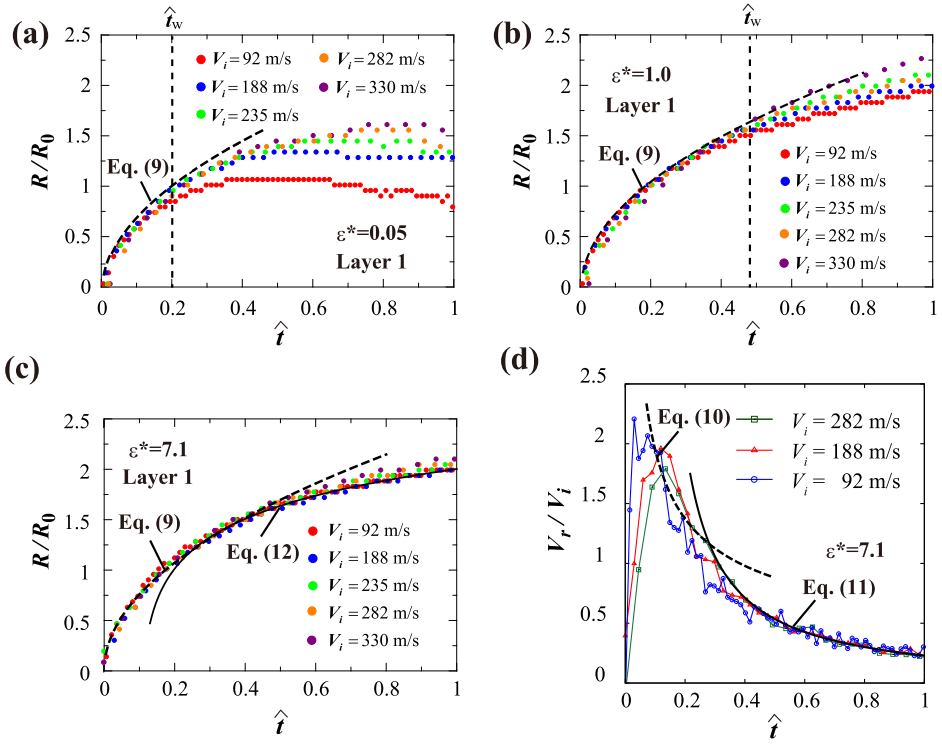

FIG. 10. Time evolutions of droplet spreading at various impact velocities (V_i = 92, 188, 235, 282, and 330 m/s): (a) Layer 1 for $\epsilon^* = 0.05$, (b) Layer 1 for $\epsilon^* = 1.0$, and (c) Layer 1 for $\epsilon^* = 7.1$. (d) Spreading velocities in Layer 1 for $\epsilon^* = 7.1$.

addition, from Eq. (9), we can easily obtain the temporal evolution of the spreading velocity for $\hat{t} < 0.3$ as follows:

$$\frac{V_r(t)}{V_i} = \frac{A'}{4}\frac{1}{\sqrt{\hat{t}}}, \quad \text{for} \quad \hat{t} < 0.3. \tag{10}$$

The droplet spreading during the time period just after the instance of the impact is also described by Eq. (7) for $\epsilon^* = 7.1$ as shown in Fig. 5(a). It should be noted here that, in Fig. 10(d), we cannot have the accurate velocity of $V_r(t)/V_i$ in $\hat{t} < 0.05$ because the ensemble average near the center of the droplet is less accurate due to the cylindrical control volume shape. However, the droplet spreading within $\hat{t} < 0.3$ can be described by Eq. (9).

For $0.3 < \hat{t} < 1.0$, we find that the time evolution of $V_r(t)/V_i$ is inversely proportional to $\hat{t}$ and based on the results presented in Fig. 10(d) is given by

$$\frac{V_r(t)}{V_i} = \frac{A''}{2}\left(\hat{t} - B''\right)^{-1}, \quad \text{for} \quad 0.3 < \hat{t} < 1.0, \tag{11}$$

where $A'' = 9/40$ and $B'' = 1/10$. The above equation is shown in Fig. 10(d) as the solid line: it is clear that the equation is well fitted for $0.3 < \hat{t} < 1.0$. In addition, the droplet spreading radius $R(t)$ in Layer 1 can be easily obtained from Eq. (11) as follows:

$$\frac{R(t)}{R_0} = A''\log(\hat{t} - B'') + C'', \quad \text{for} \quad 0.3 < \hat{t} < 1.0. \tag{12}$$

This equation is shown in Fig. 10(c), and it is clear that Eq. (12) describes this simulation result well.

Our results show that, in the case of large value of ϵ^*, the temporal evolution of the droplet spreading in Layer 1 is independent of the impact velocity within $\hat{t} \le 1.0$, in which dimensionless similarity of the spreading can be achieved. Furthermore, $V_r(t)/V_i$ can be expressed as $V_r(t)/V_i \sim 1/\sqrt{\hat{t}}$ within $\hat{t} < 0.3$ and $V_r(t)/V_i \sim \hat{t}^{-1}$ for $0.3 < \hat{t} < 1.0$, leading to $R(t)/R_0 \sim \sqrt{\hat{t}}$ and $R(t)/R_0 \sim \log\hat{t}$, respectively. In general, a wall–liquid intermolecular force is stronger than a liquid–liquid intermolecular force. Hence, it is expected in most of the cases that the values of ϵ^* are bigger

than unity. While the velocity $V_r(t)/V_i$ continuously changes with time and the power of V_r/V_i may change from $-1/2$ to -1, especially for $0.2 < \hat{t} < 0.4$, the droplet spreading due to the impact can be accurately estimated by using the above equations in the case of the large value of ϵ^*.

The effect of the temperature increase due to the high-speed impact may arise after the early stage of the droplet impact. Also, in this simulation, the effects of inertia and the wettability for nanoscale droplet spreading cannot be distinguished as shown in the previous experiment.[20] A more detailed study for the effect of inertia and the wettability is the future work.

IV. CONCLUSIONS

In the present study, we investigated nanodroplet spreading at the early stage after the impact. The simulations were conducted by changing the magnitude of intermolecular force between the liquid (Ar) and wall (Pt) molecules. The temporal evolution of the spreading diameters was measured by the cylindrical control volume for molecular layers (Layers 1–4) on the wall.

The results showed that, at the early stage of the nanodroplet impact, the normalized spreading radius of the droplet in Layer 1 is proportional to the square root of the normalized time regardless of either the intermolecular force between the liquid and wall or the impact velocity. This result is understood by the geometrical consideration presented by Rioboo *et al.*[2] and relates to the kinematic phase of the present study.

We also found that as the layer departs further from the wall, the time neglecting the effect of the wall for the droplet spreading becomes longer, and as the magnitude of the intermolecular force between the liquid and wall becomes larger, the normalized spreading diameter in Layer 1 is still independent of the impact velocity. Furthermore, the power law index of the time evolution of the spreading velocity changes from $-1/2$ to -1 with time in the case of $\epsilon^* = 7.1$.

[1] A. H. Lefebvre, *Atomization and Sprays* (Taylor & Francis, USA, 1988).
[2] R. Rioboo, M. Marengo, and C. Tropea, "Time evolution of liquid drop impact onto solid, dry surfaces," Exp. Fluids **33**, 112 (2002).
[3] A. L. Yarin, "Drop impact dynamics: Splashing, spreading, receding, bouncing," Annu. Rev. Fluid Mech. **38**, 159 (2006).
[4] C. W. Visser, P. E. Frommhold, S. Wildeman, R. Mettin, D. Lohse, and C. Sun, "Dynamics of high-speed micro-drop impact: Numerical simulations and experiments at frame-to-frame times below 100 ns," Soft Matter **11**, 1708 (2015).
[5] A. L. Biance, C. Clanet, and D. Quere, "First steps in the spreading of a liquid droplet," Phys. Rev. E **69**, 016301 (2004).
[6] J. X. Yang, J. Koplik, and J. R. Banavar, "Molecular dynamics of drop spreading on a solid surface," Phys. Rev. Lett. **67**, 3539 (1991).
[7] T. D. Blake, A. Clarke, J. De Cninck, M. De Ruijter, and M. Voue, "Droplet spreading: A microscopic approach," Colloids Surf., A **149**, 123 (1999).
[8] X. Wu, N. Phan-Thien, X. J. Fan, and T. Y. Ng, "A molecular dynamics study of drop spreading on a solid surface," Phys. Fluids **15**, 1357 (2003).
[9] G. He and N. G. Hadjiconstantinou, "A molecular view of Tanner's law: Molecular dynamics simulations of droplet spreading," J. Fluid Mech. **497**, 123 (2003).
[10] N. Sedighi, S. Murad, and S. K. Aggarwal, "Molecular dynamics simulations of nanodroplet spreading on solid surfaces, effect of droplet size," Fluid Dyn. Res. **42**, 035501 (2010).
[11] K. G. Winkels, J. H. Weijs, A. Eddi, and J. H. Snoeijer, "Initial spreading of low-viscosity drops on partially wetting surfaces," Phys. Rev. E **85**, 055301 (2012).
[12] J. Koplik and R. Zhang, "Nanodrop impact on solid surfaces," Phys. Fluids **25**, 022003 (2013).
[13] R. Zhang, S. Farokhirad, T. Lee, and J. Koplik, "Multiscale liquid drop impact on wettable and textured surfaces," Phys. Fluids **26**, 082003 (2014).
[14] X. Li, X. Zhang, and M. Chen, "Estimation of viscous dissipation in nanodroplet impact and spreading," Phys. Fluids **27**, 052007 (2015).
[15] G. Nagayama, T. Tsuruta, and P. Cheng, "Molecular dynamics simulation on bubble formation in a nanochannel," Int. J. Heat Mass Transfer **49**, 4437 (2006).
[16] D. T. Semiromi and A. R. Azimian, "Molecular dynamics simulation of nanodroplets with the modified Lennard-Jones potential function," Heat Mass Transfer **47**, 579 (2010).
[17] P. Yi, D. Poulikakos, J. Walther, and G. Yadigaroglu, "Molecular dynamics simulation of vaporization of an ultra-thin liquid argon layer on a surface," Int. J. Heat Mass Transfer **45**, 2087 (2002).
[18] H. Yaguchi, T. Yano, and S. Fujikawa, "Molecular dynamics study of vapor–liquid equilibrium state of an argon nanodroplet and its vapor," J. Fluid Sci. Technol. **5**, 180 (2010).
[19] K. K. Haller, Y. Ventikos, D. Poulikakos, and P. Monkewitz, "Computational study of high-speed droplet impact," J. Appl. Phys. **92**, 2821 (2002).
[20] C. Antonini, A. Amirfazli, and M. Marengo, "Drop impact and wettability: From hydrophilic to superhydrophobic surfaces," Phys. Fluids **24**, 102104 (2012).